AIAA JOURNAL
Vol. 41, No. 10, October 2003

# Micromechanical Analyses of Instabilities in Braided Glass Textile Composites

Shu Ching Quek* and Anthony M. Waas†
*University of Michigan, Ann Arbor, Michigan 48109-2140*

**The results of a finite element (FE)-based study of the multiaxial compressive instabilities in two-dimensional triaxial braided glass fiber composites are discussed. The micromechanics-based study was carried out on a two unit-cell size three-dimensional FE model. Computational simulations were carried out first to determine the orthotropic elastic engineering constants. The results were validated by comparison against available experimental data. Subsequently, the uniaxial compressive response and the biaxial tension/compression response of the micromodel were established using an arc-length method in conjunction with the ABAQUS commercial FE code. The approach is different from those reported in the literature where classical methods based on the technique of homogenization are used to model the elastic and inelastic response of braided composites. Instead, explicit account of the braid microstructure (geometry and packing) and the measured inelastic properties of the matrix (both the virgin properties and the in situ properties) are accounted for via the use of the FE method. This detail is necessary for developing a mechanism-based failure prediction capability. The computational model provides a means to assess the compressive and biaxial strength of the braided composites and its dependence on various microstructural parameters. It also serves as a tool to assess the most significant parameters that affect compressive strength.**

## I. Introduction

BRAIDED textile composites are alternatives to continuous fiber prepreg-based laminated composites in the aerospace and automotive industries for situations that require net shape manufacturing. Consequently, the deformation response of such composites constitutes an important area of current and continuing research. Since the early 1980s, a considerable amount of literature dealing with braided composites has been reported in the open literature. Whitcomb and Noh,[1] Naik and Stembekar,[2] Huang,[3] Naik,[4] Cox and Dadkhah,[5] and Marrey and Sankar,[6] have proposed models to predict the elastic moduli of textile composites in general. Tensile failure mechanisms and the effect of stitching on mechanical performance has been addressed by Harte and Fleck,[7] and Dow and Dexter,[8] respectively. A concise summary of developments and modeling contributions are reported by Chou[9] and Miravette.[10] Many of the previous mechanical models for braided textiles, which were focused on stiffness prediction, were based on the concept of using a smallest representative repeat unit (unit cell) that describes the architecture of the textile composite and proceeding to use suitable averaging schemes, appropriate to achieving a desired end result. The approaches used were dependent on the method of unit-cell discretization and also on the particular averaging scheme that was used to define the required macroscopic unit-cell property.

An alternate procedure that can be used to eliminate some of the dependency (on the particular method used) is to base the definition of macroscopic properties on the measured (actual) geometrical and mechanical properties of the textile composites' constituents. The solution of the boundary-value problems thus posed are obtained by resorting to a numerical technique, such as the finite element method.

In the present paper, the response and failure of glass two-dimensional triaxial braided composites (2DTBC) are studied via the finite element method. Two micromodels (micromodel A and micromodel B) incorporating measured geometry and nonlinear material properties were created using the commercial software SDRC-IDEAS Master Series 8. The differences in the two micromodels are related to the manner in which initial geometrical imperfections associated with the 0-deg tow are modeled. In micromodel A, the zero fiber tow is modeled as a straight elastic tow, whereas in micromodel B, the zero fiber tow is modeled as an undulating elastic tow with the undulations based on measured geometry. Three-dimensional solid elements are used for the tows and the matrix material. The modeling was motivated by a need to capture experimentally observed compressive failure mechanisms that consisted of details at the 2DTBC unit cell level. The response of the micromodels under uniaxial and multiaxial loading conditions was established using the RIKS arc-length method,[11,12] option available in ABAQUS. An approach similar to this has been previously used successfully for the study of compressive failure and compressive strength of continuous fiber-laminated composites by Ahn and Waas[13] for notched multidirectional laminated composites and by Lee and Waas[14] for unnotched unidirectional composites. In the present paper, the predictions of the computational model for the multiaxial compressive strength of braided composites and the dependence of strength on tow misalignments are presented and discussed.

## II. Properties and Architecture of the Glass Triaxially Braided Composite

### A. Macroscale Measurements

Using the American Society for Testing and Materials (ASTM) D 3039 standard, uniaxial tensile tests were performed to obtain the macroscopic orthotropic moduli and response. For each test, three samples were used to ensure accuracy, and the average of the test data for orthotropic engineering constants are reported in this paper. Separate tests were conducted to obtain the virgin and in situ matrix properties of the braided glass composites. The in situ matrix properties will be discussed later. The braided −30/0/+30 deg glass fiber polyvinylester composite (E glass) is from Owens Corning; the resin is Dow Spectrum MM364 isocyanurate with three plies, 5 mm (0.214 in.) thick with a volume fraction of 45%. Table 1 shows measured engineering constants of the glass 2DTBC.

### B. Microscale Measurements

To observe the braided tows of glass fibers more easily, the braided mat (dry preform) without the resin is shown in Fig. 1. The outlined

Received 24 December 2002; revision received 15 May 2003; accepted for publication 19 May 2003. 

*Graduate Research Assistant, Aerospace Engineering Department, Composite Structures Laboratory.

†Professor, Aerospace Engineering Department, Composite Structures Laboratory; dcw@umich.edu. Associate Fellow AIAA.

**Table 1 Elastic engineering constants of glass 2DTBC**

| Properties | Experimental data |
|---|---|
| $E_z$, GPa (Msi) | 12.89 (1.87) |
| $E_x$, GPa (Msi) | 27.18 (3.94) |
| $G_{xz}$, GPa (Msi) | 6.70 (1.00) |
| $\nu_{xz}$ | 0.33 |

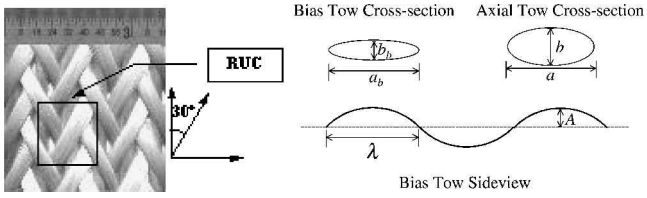


**Fig. 1 Dry glass braid perform with boundary of RUC.**

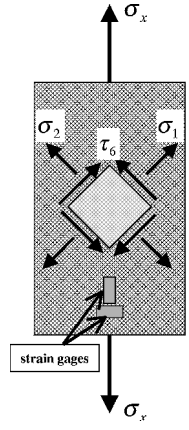


**Fig. 2 Schematic diagram of test section used in determining in situ matrix properties: $\sigma_1 = \sigma_x/2 + \tau_{xy}$, $\sigma_2 = \sigma_x/2 - \tau_{xy}$, $\tau_6 = \sigma_x/2$, $\varepsilon_1 = \varepsilon_2 = (\varepsilon_x + \varepsilon_y)/2$, and $\gamma_6 = \varepsilon_x - \varepsilon_y$.**

area is the representative unit cell (RUC) found within the triaxial braids. Bias tows are woven at 30 deg to the vertical axis. At least six measurements were made throughout the mat to obtain average values of each key dimension used to reconstruct the glass 2DTBC microstructure for the purpose of finite element (FE) modeling. The key dimensions consist of the wavelength $2\lambda$, amplitude $A$, axial tow cross-sectional dimensions $a \times b$, and bias tow cross-sectional dimensions $a_b \times b_b$ (Fig. 2). For the $-30/0/+30$ deg glass TBC used, $\lambda = 14.030$ mm, $A = 0.701$ mm, $a \times b = 3.012 \times 0.503$ mm, and $a_b \times b_b = 3.010 \times 0.498$ mm. The tows are assumed to have an elliptical cross section, and this assumption has been verified via scanning electron microscope images.

## III. FE Modeling of RUC

Several approaches can be used to establish the composite mechanical properties at the macroscopic level. Volume-averaging schemes, as described by Nemat-Nasser and Hori,[15] for example, provide relations between macroscopic stresses and macroscopic strains. Implicit in volume-averaging approaches is the assumption that the composite material is homogeneous (at the scale of the RUC) in nature, and thus, the instantaneous (tangent) moduli obtained are averaged over the volume of the particular RUC. This implies that no local information will be available inside the RUC of the composite. Such homogenized approaches do not provide constituent stresses and strains within the unit cell. These local quantities are needed for implementing failure criteria for experimentally observed failure mechanisms such as fiber/tow debonding and fiber tow buckling. In the present study, explicit account of the microstructure of the 2DTBC is taken into consideration to implement a FE-based solution to understand the experimentally observed failure mechanism of tow buckling.

### A. Creation of Micromodel

The micromodels in the present work were built using the commercial software package SDRC-IDEAS Master Series 8. Because of the complexity of the geometry, a sophisticated CAD tool and a FE meshing tool is required. The microarchitecture of the 2DTBC is shown in Fig. 3.

**Table 2 Properties of constituents**

| Material | $E$, GPa | $G$, GPa | $\nu$ |
|---|---|---|---|
| Matrix[a] | 5.0 | 1.83 | 0.36 |
| Fibers[b] | 72.4 | 29.67 | 0.22 |

[a]Epoxy (Dow Spectrum MM364).
[b]E glass (Owens Corning).

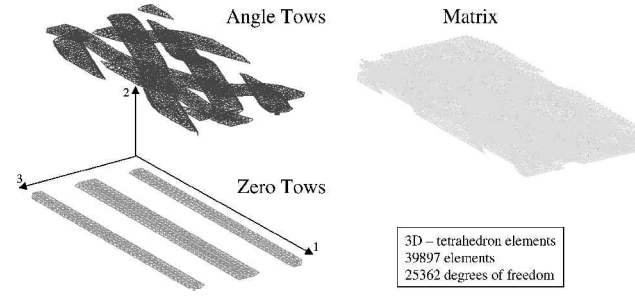


**Fig. 3 FE model of $-30/0/+30$-deg glass TBC.**

The adequacy of the FE mesh was verified via comparison of the micromodel mechanical properties with measured experimental data. The size of elements used for meshing (and, thus, the mesh density) was controlled by the gaps and spaces of the actual braid architecture. Consequently, the smallest element size was set by the minimum spacing between the tows and the matrix at certain locations within the RUC. The spacing between the zero tows and bias (angle) tows were such that element dimensions less than 0.02 mm could not be used to generate the mesh. To have matching boundaries between one segregated volume and another, similar element sizes had to be used. To accommodate this element size issue, the results presented were generated with an optimal mesh density that is sufficiently fine, to not create severe element distortion errors and violate small geometrical clearances. The results presented here are with the finest of meshes that permit a FE solution without inducing such numerical errors. Further refinement of the mesh leads to local artifical stiffening rendering a nonconvergent solution.

### B. Assumptions Made During Modeling of the Microstructure

Table 2 shows the properties of glass fibers and the epoxy matrix. To create the micromodel of the $-30/0/+30$ deg 2DTBC, several assumptions had to be made. The tows were treated as one entity with the assumption of transverse isotropy. That is, the tows are assumed to be three-dimensional space undulating curved beams. The tow properties were generated using the values in Table 2. Tow cross-sectional area adjustments were made when a smaller value was used due to geometrical constraints associated with clearances imposed during the FE modeling of the microstructure. This was necessary to provide a larger than actual spacing between the axial tows and the bias tows. As such, the element size for the matrix need not be so small that the model will end up having too many elements that cannot be handled by the present available computational power. The tow area adjustments were made such that the axial stiffness of the tows was preserved. That is, area adjustments were made according to

$$E_1^* = \left(A_1 / A_1^*\right) E_1 \tag{1}$$

where $E_1$ is the original modulus corresponding to $A_1$. A superscript asterisk corresponds to the corrected modulus corresponding to the new area. Other composite tow properties are based on a maximum allowable fiber volume fraction associated with the hexagonal packing of circular cross-sectional fibers. Thus, $V_f = 90\%$, was assumed in the tows. The transversely isotropic composite tow properties were computed by using the Halpin–Tsai relations as given by Herakovich.[16]

To obtain the compressive response of the initially imperfect 2DTBC, nonlinear constitutive properties of the matrix are required

for finite deformation. For this purpose, the virgin matrix material is modeled as an elastic–plastic solid obeying J2 incremental flow theory of plasticity with a von Mises yield criterion and an associated flow rule (see Ref. 17). The nonlinear uniaxial response of the virgin matrix material was measured and used first in conjunction with the FE simulations in ABAQUS for uniaxial response analysis using micromodel A. Subsequently, for the biaxial analyses with micromodel A and for all analyses with micromodel B, the approximate measured in situ properties of the matrix material (see next section) were used in the FE simulations.

### C. In Situ Matrix Properties

It has been shown before that the in situ response of the polymer matrix in a braided composite has effective properties that are different than the virgin resin material (Yerramalli and Waas[18] and the references contained therein). This is due to (unwanted) residual stresses and heterogeneity of properties caused by matrix curing in a nonuniform temperature distribution because of the presence of fiber tows. The regions of matrix that are located at the boundary between the tow and matrix undergo a different thermal history than the bulk matrix, thus, inducing an interphase.[18] The presence of interphases and residual stresses can be accounted for by modeling the matrix as a new material with an effective stress–strain relation that indirectly accounts for these effects. Such an effective characterization is referred to as an in situ matrix stress–strain relation. In the present work, the in situ stress–strain relation of the matrix material in the braided composite is approximately obtained by using a test specimen that has straight fibers but is cured under the same conditions as that of the braided composite. Although it is true that the initial residual stress state in a braided composite may differ from that of a continuous straight fiber composite laminate, it is assumed that the differences are small because the matrix properties are influenced most by the interphase. The interphases are governed by thermal mismatch, and because the same fibers and matrix are used in both the braided composite and the continuous fiber composite laminate, the interphase regions in both are likely to have the same level of heterogeneity. The ASTM D 3039 standard uniaxial test was conducted on a $(-45/+45)_8$-deg continuous fiber-composite laminate made from the same resin and cured under the same thermal history as that of the braided composite. Strain gauges were placed as shown in Fig. 2.

A shear stress vs shear strain plot of the composite is generated from the results obtained from this test, as explained by Herakovich.[16] From these data, the tangent shear modulus can be computed as a function of shear stress. Using the Halpin–Tsai relations, as given by Herakovich,[16] and after some manipulation, we obtain the relation between the tangent shear modulus of the in situ matrix and the composite tangent shear modulus as

$$G_m = G_{12}\frac{(G_{12f}+G_m)-\upsilon_f(G_{12f}-G_m)}{(G_{12f}+G_m)+\upsilon_f(G_{12f}-G_m)} \tag{2}$$

Integrating these data provides the shear response data for the matrix. These shear response data, in conjunction with the J2 incremental theory of plasticity, can be used to construct the effective stress-effective plastic strain relation that is needed as input data for the ABAQUS simulation. Figure 4 shows the results obtained for the in situ matrix shear response, and Fig. 5 shows the difference between the virgin matrix and the experimentally obtained in situ matrix response. The virgin matrix properties were used in micromodel A for the uniaxial response simulations, and the in situ matrix properties were used for the biaxial simulations. The in situ matrix properties were used throughout in micromodel B simulations. The effect this has on the response of each micromodel is presented in the "Results and Discussion" section.

### D. Boundary Conditions of Micromodel and Imperfections Imposed

The first micromodel (micromodel A) consists of two unit cells. Planar (two-dimensional) views of micromodel A and the loading under displacement control conditions used to obtain the linear elastic response (and the corresponding orthotropic engineering

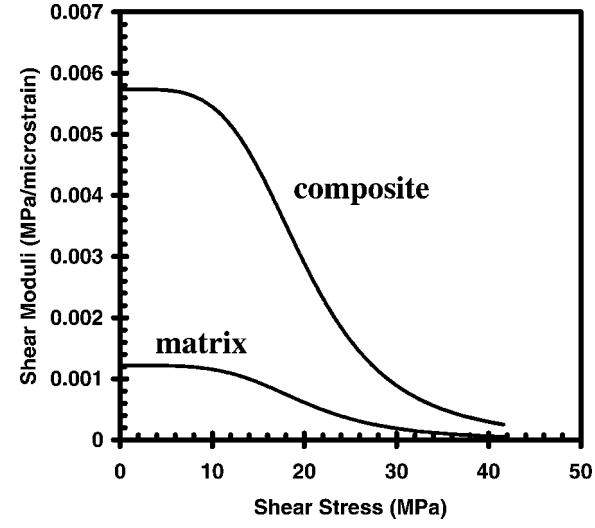


**Fig. 4 Shear modulus vs shear stress for in situ matrix and −30/0/+30-deg glass braided composite.**

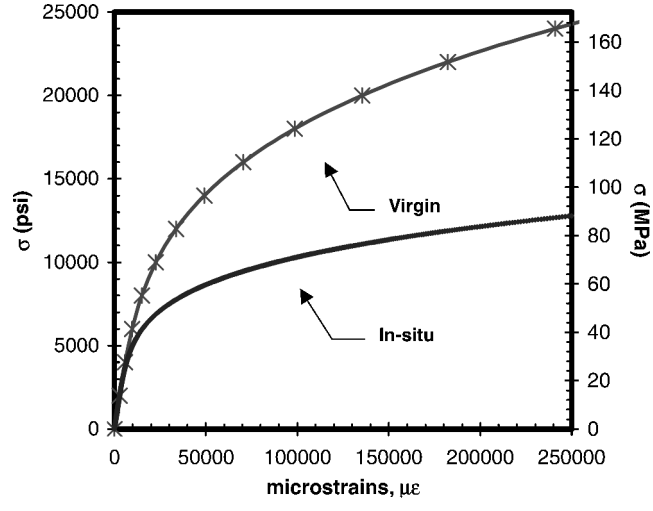


**Fig. 5 Uniaxial stress–strain curve of matrix used in FE model.**

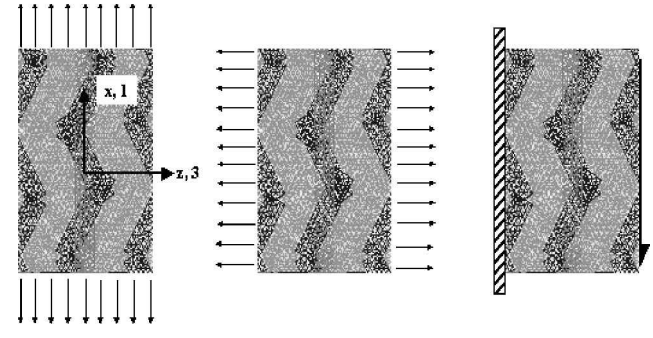


**a) Tension displacement control, one direction** **b) Tension displacement control, three direction** **c) Shear displacement control 1–3 plane**

**Fig. 6 Loading conditions for obtaining elastic moduli.**

constants) are as shown in Fig. 6. For the response analysis using the RIKS arc-length method, results were first obtained for uniaxial compression in the $x$ direction. Several response analyses were conducted on a series of imperfect micromodels. The imperfections were generated by first deforming micromodel A by a small known amount. This was done by displacing the points L and M of the end face EFGH (Fig. 7) by an amount $\delta$ in the $y$ and $z$ directions. During this step, points J and K of face ABCD are held fixed, while all other nodes of the micromodel are left unconstrained. Each value of

$\delta$ produces an imperfect micromodel. Because the 0-deg tow is lying along the $x$ direction, this initial load step provides a misalignment of the main 0-deg tow. Next, a response analysis for each imperfect micromodel was carried out. During the response analyses, all nodes of face ABCD are restrained from motion in the $x$ direction, while points J and K are fixed. Points M and L are fixed in the $y$ and $z$ directions, while the nodes on the face EFGH are specified to move only in the negative $x$ direction.

The response of micromodel A to biaxial proportional loading was also investigated. For the uniaxial compression loading case, initially, micromodel A was deformed by a small known amount. This was done by displacing points L and M of the end face of EFGH (Fig. 7) by 0.004 mm in the $y$ and $z$ directions. During this step, points J and K of face ABCD are held fixed. Next, a response analysis was carried out in a proportional manner. When this is done, faces EADH, FBGC, EFGH, and ABCD remain flat in the deformed configuration. Faces EADH and FBGC remain parallel to each other after deformation, and the same is true for faces ABCD and EFGH. Several proportional compressive/tensile load paths were studied. Results obtained from these studies are presented in the next section.

Thus far, the mentioned imperfections (in micromodel A, where the 0-deg tow is straight) are what we refer to as induced imperfections because the 0-deg tow is built into the micromodel as a perfectly straight transversely isotropic beam. The second micromodel (micromodel B) consisted of a one unit-cell RUC, with the geometrical undulations of the zero tow built into it. The magnitude and shape of the geometrical imperfections used in the micromodel were obtained via measurements from optical microscopy images as shown in Fig. 8 with the horizontal line as a reference line. The imperfections (in terms of axial tow undulations) are about 0.15–0.20 mm in amplitude. Figure 9 shows the FE model with a built in imperfection of 0.16 mm. This model was subjected to the same uniaxial and biaxial loading histories as described earlier for micromodel A.

## IV. Results and Discussion

### A. Elastic Engineering Constants Verification of Micromodel

Table 3 shows the comparison between experimental and computational results for the orthotropic elastic engineering constants. The computational results obtained (for both micromodels A and B) are in close agreement with the measured experimental values. Note that the experimental uniaxial specimens contain several unit cells in the gauge section, and the close agreement between experiment and the predictions from the micromodels attests to the homogeneous deformation assumption, implicit in the measurement of properties through a uniaxial ASTM D 3039 standard test. The results for engineering constants obtained via the computational micromodels rely on definitions of macroscopic stress and macroscopic strain that are based on the micromodel. For example, for the determination of $E_x$ through the FE simulations, the macroscopic stress $\Sigma_x$ is defined as the sum of reaction forces on face ABCD divided by the area ABCD, and macroscopic strain $\varepsilon_x$ is defined as total elongation of the unit cell divided by the length in the direction of elongation. The good correlation between computation and measurement points to an increased level of confidence in the meshing and construction of the micromodel, as well as to the accuracy of the assumptions made regarding simplifications to the modeling of the tows.

### B. Instabilities in a −30/0/+30-Degree Glass 2DTBC

Accurate predictions of the elastic engineering constants provide verification of the computational model. As explained earlier, a two-step approach was used to carry out the compressive response analysis of the micromodels using the RIKS method option in ABAQUS. For micromodel A, these steps consisted of introducing a misalignment to the 0-deg tow (or the axial tow) as explained earlier, followed by a response analysis, using nonlinear geometry and nonlinear matrix material properties in conjunction with the RIKS arc-length following method.

The results obtained from the uniaxial compressive response study of micromodel A for a series of different induced imperfection magnitudes are plotted in Fig. 10. The uniaxial compressive response of micromodel A predictions can be understood by examining a typical $\Sigma_x$ vs $\varepsilon_x$ plot for a given initial imperfection magnitude $\delta$. Initially, all of the micromodel A responses display a relatively stiff linear behavior. The magnitude of the slope of this

**Table 3 Computational model prediction of elastic engineering constants**

| Properties | Experimental data | Computational data | % Error |
|---|---|---|---|
| $E_x$, GPa (Msi) | 12.89 (1.87) | 12.44 (1.80) | −3.49 |
| $E_z$, GPa (Msi) | 27.18 (3.94) | 26.92 (3.90) | −0.96 |
| $G_{xz}$, GPa (Msi) | 6.70 (1.00) | 5.42 (0.77) | −19.0 |
| $\nu_{xz}$ | 0.33 | 0.34 | +2.9 |

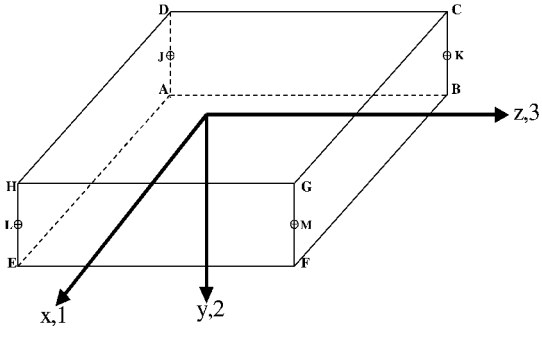


**Fig. 7 Boundary location of micromodel where displacement constraints are applied.**

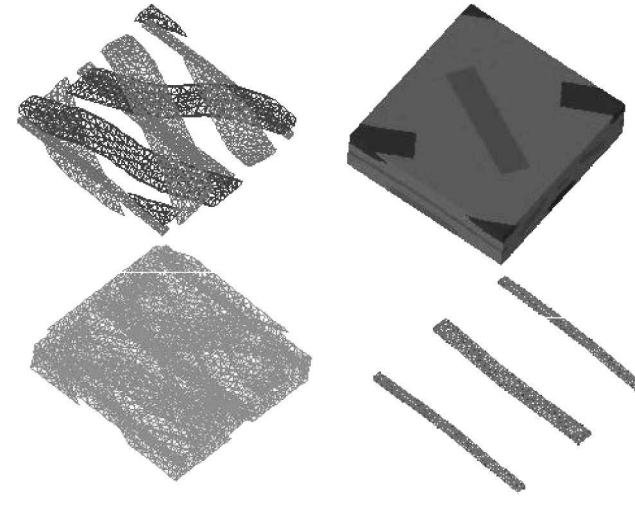

**Fig. 9 FE model of the RUC for glass 2DTBC with built in imperfections in the axial tows.**


**Fig. 8 Microscopic image of the axial tow undulations in a glass 2DTBC specimen: 4.93 mm (0.194 in.) thickness with 0.15–0.22-mm undulation.**

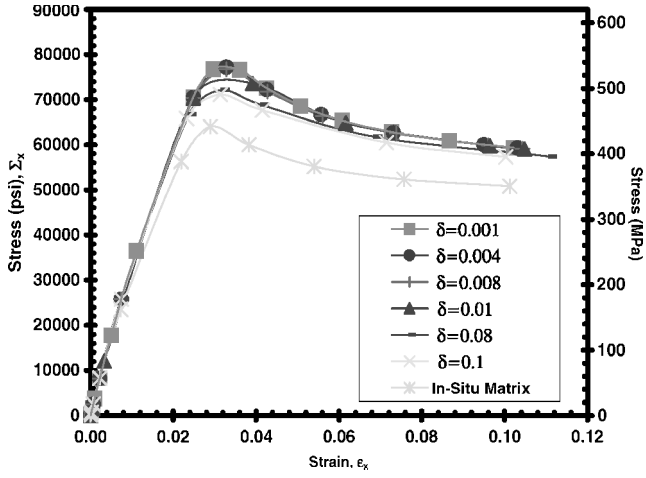


**Fig. 10 Macroscopic stress–strain relationship under influence of different induced imperfections for micromodel A.**

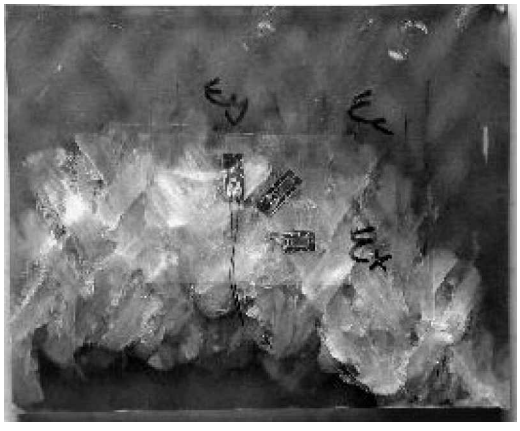

**Fig. 11 Typical tow buckling phenomenon seen in compression tests; whitening of matrix due to distributed matrix cracking and fiber/matrix debonding.**

line for all of the imperfect micromodels is 27 GPa and agrees well with the tensile experimental data.

As seen in Fig. 10, with continued loading, the micromodel response becomes progressively nonlinear, and at a strain $\varepsilon_x$ of approximately 0.035, a maximum stress $\Sigma_x$ of 72,000 psi (496 MPa) is reached (for a micromodel with an induced imperfection magnitude of 0.01 mm). The value of strain at this maximum or peak and the value of the corresponding stress itself are dependent on the magnitude of $\delta$, which is associated with the degree of misalignment of the 0-deg tow. The progressive reduction in the macroscopic stiffness of micromodel A is due to the geometrical nonlinearity associated with the bias tows and the main 0-deg tow, as well as with the material nonlinearity of the matrix. Indeed, as loading proceeds, the matrix material that is between the tows is required to support increasing amounts of shear stress. However, the equivalent stress-strain curve of the matrix indicates that the matrix modulus decreases progressively as the stress increases. Thus, because of the interaction of these nonlinearities, the overall stiffness of the micromodel progressively decreases, leading to a limit-load type of instability. In an experimental setting, this limit load can be interpreted as the maximum compressive strength of the composite. However, at this load (or even before this), other events, such as matrix cracking and separation of the tows from the matrix (matrix/tow debonding) can occur, which may lead to the surface angle tows popping out, as is characteristically seen in a compression experiment at failure (Fig. 11). The modeling of matrix cracking and tow/matrix separation requires knowledge of the matrix cracking toughness and the tow/matrix interface toughness. Because reliable data pertaining to these mechanisms are currently not available, they are not

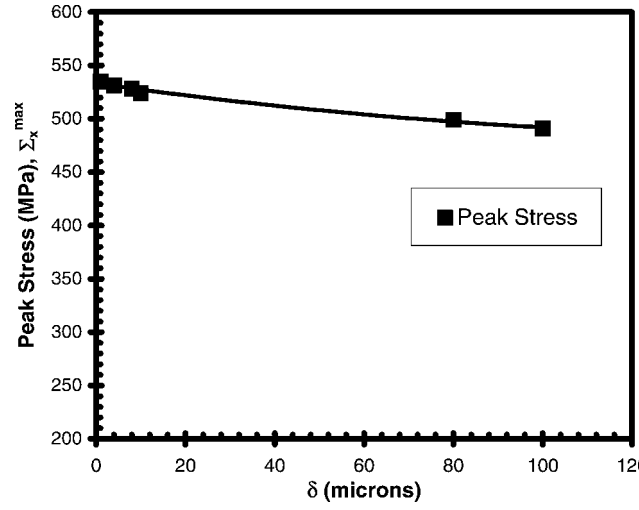


**Fig. 12 Relationship between imperfection magnitude $\delta$ (micrometers) and peak stress (megapascal) for micromodel A.**

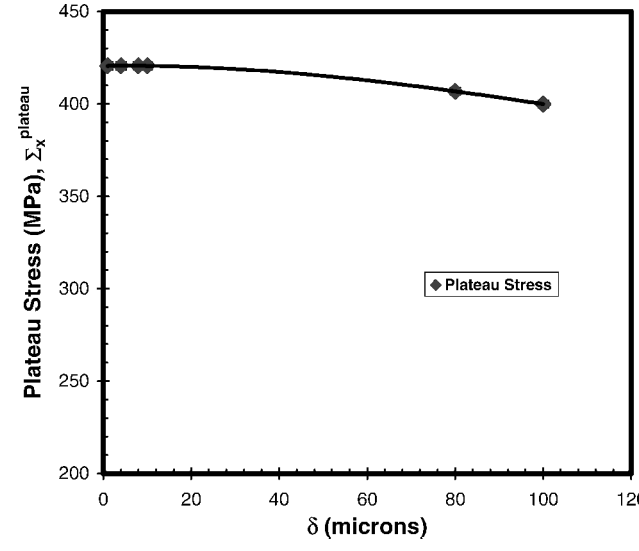


**Fig. 13 Relationship between imperfection magnitude $\delta$ (micrometers) and plateau stress (megapascal) taken at 9% strain, for micromodel A.**

considered in the present study. Instead, matrix distributed cracking, for instance, is being modeled through the elastic–plastic stress–strain response of the matrix with the implicit assumption that such cracking induces plasticlike behavior. A cohesive zone approach, as described by Shahwan and Waas,[19] is being currently considered for tow/matrix separation and is the subject of a separate study.

As seen in Fig. 10, subsequent to the limit load, the axial stress is seen to diminish along with increasing amounts of axial strain. (Actually it is possible for both the stress and the strain to decrease simultaneously, due to the arc-length tracing RIKS method that is adopted in the solution process in ABAQUS.) Thus, the present micromodel A response is stable under displacement control conditions. Eventually, the rate of decrease of stress levels off to a near constant plateau stress. All of the results presented with micromodel A used the virgin material properties. The effect of using the in situ matrix properties is shown in Fig. 10, where the $\Sigma_x - \varepsilon_x$ curve for an induced imperfection corresponding to $\delta = 0.004$ with in situ matrix properties is shown. Both the limit load and plateau load are seen to be lowered with the use of the in situ matrix properties. Consequently, in all subsequent simulations (biaxial simulations with micromodel A and uniaxial and biaxial simulations with micromodel B), the in situ matrix behavior is used.

Figure 12 shows the change of maximum stress as a function of imperfection magnitude for uniaxial response predictions with micromodel A, and Fig. 13 shows the corresponding plateau stress

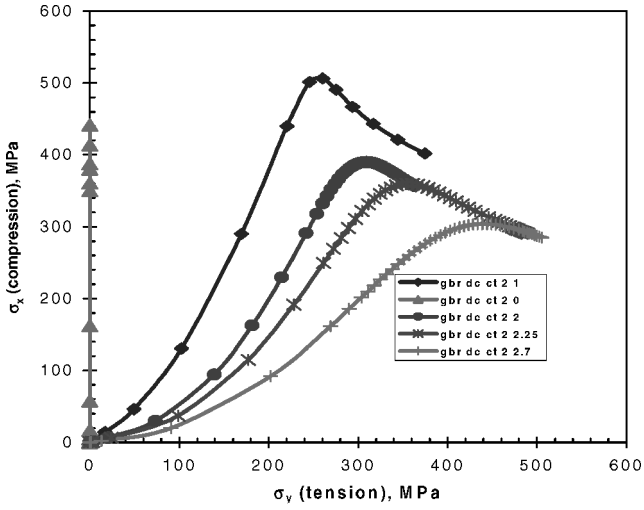


**Fig. 14 Compressive stress $\sigma_x$ vs tensile stress $\sigma_y$ response for uniaxial and biaxial displacement control proportional loading, micromodel A.**

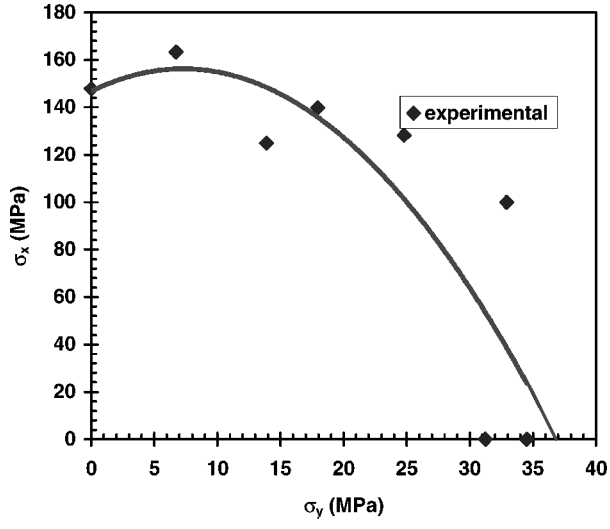


**Fig. 15 Experimental failure envelope for glass braided composite +30/0/−30 deg.**

behavior. Whereas the maximum stress appears to converge, the plateau stress does not. This is because the plateau stress is continually dependent on the extent (volume) of material that undergoes damage, and with increasing stress level, larger portions of the matrix material in the micromodel are subjected to plastic straining, leading to a decrease in the effective stiffness of the matrix.

### C. Effects of Instabilities with Biaxial Loadings

Figure 14 shows the responses of micromodel A for a series of simulations under different proportional biaxial loads. As the ratio of tension to compression increases, the maximum macroscopic compressive stress (limit point) decreases and shifts toward the increasing $\sigma_y$ direction. This trend is also seen in the experiments conducted. Because there was a limited supply of glass braided composite material available, only a few biaxial compression/tension tests were conducted for obtaining the corresponding failure envelope. The details of these tests are reported in Ref. 20. The biaxial tests were carried out in a special loading fixture that is capable of applying proportional compression/tension biaxial loading in the manner that has been studied with the micromodel. Note that the tests are conducted on specimens that contain several unit cells. Figures 15 and 16 show the experimental and computational failure points, respectively. These correspond to the maximum stress deduced from the experimental results and the maximum macroscopic stress predicted from the micromodel simulations. Although

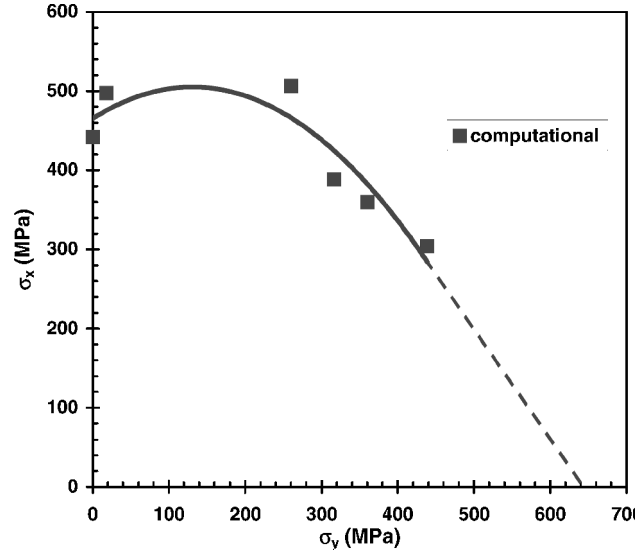


**Fig. 16 Computationally predicted failure envelope for glass braided composite +30/0/−30 deg with micromodel A.**

the curves do not match, the predicted trend for the strength envelope is observed to be the same. The reasons for the higher failure stress predicted through micromodel A simulations are discussed later.

Results obtained with micromodel B are compared against the predictions of micromodel A and experiment in Fig. 17. Recall that, in micromodel B, the zero tow initial imperfection magnitude, corresponding to measured zero tow undulations, was built into the creation of micromodel B. Thus, not surprisingly, the results obtained for the limit points for several biaxial proportional loading histories with micromodel B are in much better agreement with experiment, as shown in Fig. 17. The good agreement between prediction and experiment when using micromodel B points to the need to use realistic and accurate geometrical imperfections in compressive strength predictions of these types of 2DTBC. Clearly, if one knows the degree of undulations (obtained statistically through microscopic measurements), then it is possible to generate bounds on the expected compressive strengths. In this manner, it becomes possible to obtain, through prediction, an envelop of composite compressive strength with upper and lower bounds based on the statistics of the known zero two undulations.

Recall that the micromodel predictions captured the microstructural instability, with the loading faces constrained to remain flat during the loading process. This implies that failure is associated with all cells failing simultaneously in the experiment. As indicated in Fig. 11, the maximum compressive load is associated with deformation localization, occurring within a few cells. Thus, it is conceivable that unit-cell failure models corresponding to proportional compression/tension pressure control loading, where the faces are free to deform, would lead to even lower numerical predictions, bringing prediction and measurement to a very close agreement. This aspect warrants further study. The tows within the micromodels were assumed to be transversely isotropic and linear elastic; however, in reality these tows contain matrix materials that are stressed into the nonlinear regime. Consequently, the tows can be modeled within the framework of an appropriate transversely isotropic elastic–plastic characterization. A generalization of the Hill orthotropic elastic–plastic model as proposed by Sun and Chen[21] is being considered for this purpose. This modeling feature will also result in a lowering of the predicted compressive strength. Finally, matrix cracking occurring before tow instability should also be accounted for in the modeling of textile composites. A thermodynamically consistent damage mechanics formulation for this purpose has been proposed by Schapery[22] and recently used by Basu et al.[23] The implementation of such a formulation requires that the matrix cracking phenomenon be suitably characterized via coupon level tests.

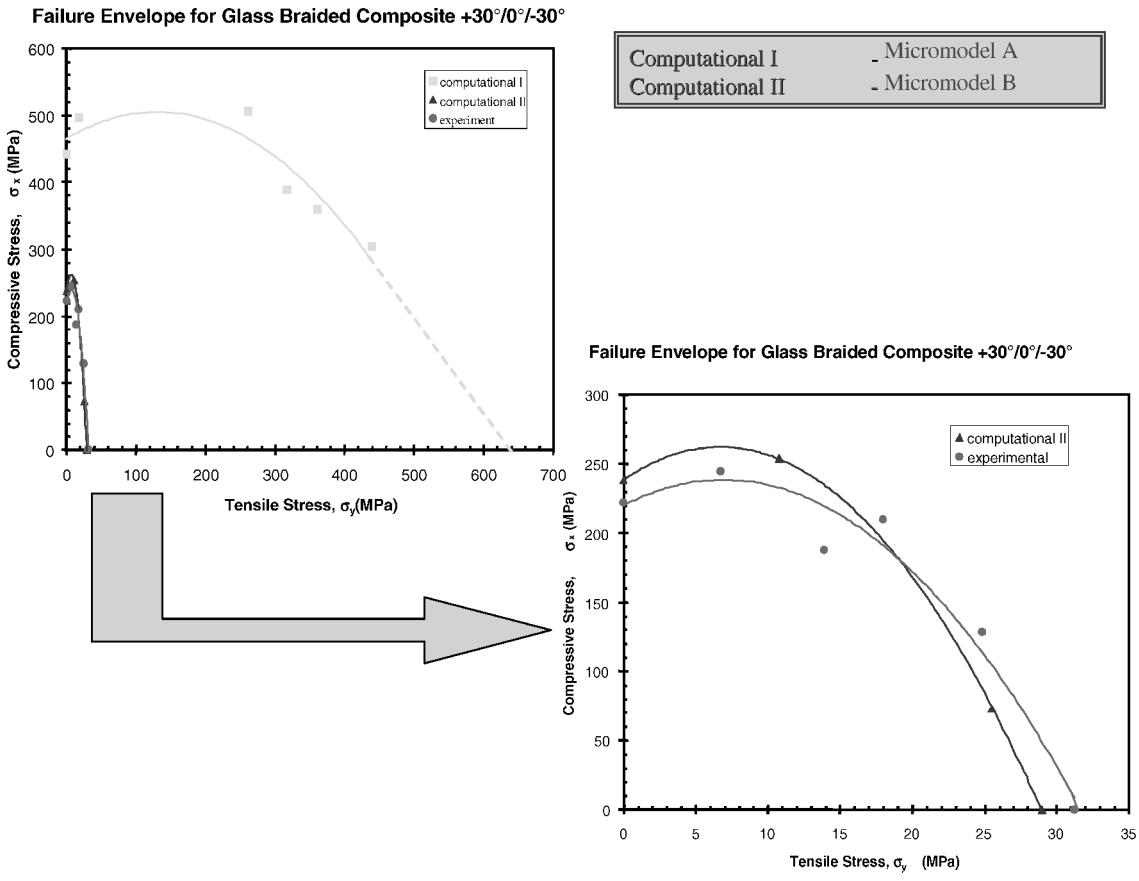


**Fig. 17 Comparison of results using micromodel A and micromodel B; latter model predictions compare well against experiment.**

## V. Conclusions

Compressive instabilities in two-dimensional triaxially braided glass fiber textile composites in a multiaxial setting have been studied. A computational model has been described and is found to be capable of predicting compressive strength of the braided composite under uniaxial compression and a variety of biaxial compression/tension loadings. Inputs to the model are fiber/tow architecture of the braid, the elastic properties of the fiber, the fiber volume fraction, and the complete nonlinear stress–strain response of the matrix. When only these inputs are used, a methodology has been presented for predicting compressive strength of the material, its dependence on tow misalignment, and stress biaxiality. The results from the unit-cell model with built in zero tow imperfections and measured in situ matrix properties compared well against experimental data. The results from the simulations show that geometrical imperfections at the microstructural level are the most significant in influencing compressive strength.

## Acknowledgments

The authors are grateful for the financial sponsorship of the Automotive Composites Consortium, Energy Management Working Group, and the Department of Aerospace Engineering, University of Michigan. The authors acknowledge that this research was supported, in whole or in part, by Department of Energy cooperative agreement DE-FC05-95OR22363. Such support does not constitute an endorsement by the Department of Energy of the views expressed herein. The interest and support of K. W. Shahwan and V. Agaram from DaimlerChrysler Corp. are gratefully acknowledged.

## References

[1]Whitcomb, J., and Noh, J., "Concise Derivation of Formulas for 3D Sublaminate Homogenization," *Journal of Composite Materials*, Vol. 34, 2000, pp. 522–535.

[2]Naik, N. K., and Stembekar, P. S., "Elastic Behavior of Woven Fabric Composites: I—Lamina Analysis," *Journal of Composite Materials*, Vol. 26, 1992, pp. 2196–2225.

[3]Huang, Z. M., "The Mechanical Properties of Composites Reinforced with Woven and Braided Fabrics," *Composites Science and Technology*, Vol. 60, 2000, pp. 479–498.

[4]Naik, R., "Analysis of 2D Triaxial and 3D Multi-interlock Braided Textile Composites," AIAA Paper 96-1530, April 1996.

[5]Cox, B. N., and Dadkhah, M. S., "The Macroscopic Elasticity of 3D Woven Composites," *Journal of Composite Materials*, Vol. 29, 1995, pp. 785–819.

[6]Marrey, R., and Sankar, B., "Analytical Methods for Micromechanics of Textile Composites," *Composites Science and Technology*, Vol. 57, No. 6, 1997, pp. 703–713.

[7]Harte, A. M., and Fleck, N. A., "The Mechanics of Braided Composites in Tension," *European Journal of Mechanics*, Vol. 19, 1999, pp. 259–276.

[8]Dow, M. B., and Dexter, H. B., "Development of Stitched, Braided and Woven Composite Structures in the ACT Program at Langley Research Center," NASA TP-97-206234, 1997.

[9]Chou, T. W., *Microstructural Design of Fiber Composites*, Cambridge Solid State Science Series, Cambridge Univ. Press, Cambridge, England, U.K., 1992.

[10]Miravette, A., *3-D Textile Reinforcements in Composite Materials*, Woodhead, 1999.

[11]Riks, E., "The Application of Newton's Method to the Problem of Elastic Stability," *Journal of Applied Mechanics*, Vol. 39, No. 4, 1972, pp. 1060–1065.

[12]Riks, E., "Incremental Approach to the Solution of Snapping and Buckling Problems," *International Journal of Solids and Structures*, Vol. 15, No. 7, 1979, pp. 529–551.

[13]Ahn, J. H., and Waas, A. M., "Prediction of Compressive Failure in Laminated Composites at Room and Elevated Temperature," *AIAA Journal*, Vol. 40, No. 2, 2002, pp. 346–358.

[14]Lee, S. H., and Waas, A. M., "Compressive Response and Failure of Fiber Reinforced Unidirectional Composites," *International Journal of Fracture*, Vol. 100, No. 3, 1999, pp. 275–306.

[15]Nemat-Nasser, S., and Hori, M., *Micromechanics: Overall Properties of Heterogeneous Materials*, Elsevier Science, Amsterdam, 1993.

[16]Herakovich, C. T., *Mechanics of Fibrous Composites*, McGraw-Hill, New York, 1998.

[17]Doghri, I., *Mechanics of Deformable Solids*, Springer-Verlag, Berlin, 2000.

[18]Yerramalli, C. S., and Waas, A. M., "In-Situ Matrix Shear Response Using Torsional Test Data of Fiber Reinforced Unidirectional Polymer Composites," *Journal of Engineering Materials and Technology*, Vol. 124, No. 2, 2002, pp. 152–159.

[19]Shahwan, K., and Waas, A. M., "Non-Self-Similar Decohesion Along a Finite Interface of Unilaterally Constrained Delamination" *Proceedings of the Royal Society of London*, Vol. 453, 1997, pp. 515–550.

[20]Quek, S. C., "Compressive Instabilities in Braided Textile Composites: Experiment and Analysis," Ph.D. Dissertation, Aerospace Engineering Dept., Univ. of Michigan, Ann Arbor, MI, Oct. 2002.

[21]Sun, C. T., and Chen, J. L., "A Simple Flow Rule for Characterizing Nonlinear Behavior of Fiber Composites," *Journal of Composite Materials*, Vol. 23, 1989, pp. 1009–1021.

[22]Schapery, R. A., "A Theory of Mechanical Behavior of Elastic Media with Growing Damage and Other Changes in Structure," *Journal of the Mechanics and Physics of Solids*, Vol. 38, No. 2, 1990, pp. 215–253.

[23]Basu, S., Waas, A. M., and Ambur, D. R., "Computational Modeling of Damage Growth in Composite Laminates," *AIAA Journal*, Vol. 41, No. 6, 2003, pp. 1158–1166.

A. N. Palazotto
*Associate Editor*